PHILOSOPHICAL TRANSACTIONS OF THE ROYAL SOCIETY A

Phil. Trans. R. Soc. A (2006) **364**, 711–723
doi:10.1098/rsta.2005.1733
Published online 25 January 2006

High-intensity laser-driven proton acceleration: influence of pulse contrast

By Paul McKenna[1,*], Filip Lindau[2], Olle Lundh[2], David Neely[3], Anders Persson[2] and Claes-Göran Wahlström[2]

[1]*SUPA, Department of Physics, University of Strathclyde, 107 Rottenrow, Glasgow G4 0NG, UK*
[2]*Department of Physics, Lund Institute of Technology, PO Box 118, 221 00 Lund, Sweden*
[3]*Central Laser Facility, Rutherford Appleton Laboratory, Chilton, Didcot, Oxon OX11 0QX, UK*

Proton acceleration from the interaction of ultra-short laser pulses with thin foil targets at intensities greater than $10^{18}\,\mathrm{W\,cm^{-2}}$ is discussed. An overview of the physical processes giving rise to the generation of protons with multi-MeV energies, in well defined beams with excellent spatial quality, is presented. Specifically, the discussion centres on the influence of laser pulse contrast on the spatial and energy distributions of accelerated proton beams. Results from an ongoing experimental investigation of proton acceleration using the 10 Hz multi-terawatt Ti : sapphire laser (35 fs, 35 TW) at the Lund Laser Centre are discussed. It is demonstrated that a window of amplified spontaneous emission (ASE) conditions exist, for which the direction of proton emission is sensitive to the ASE-pedestal preceding the peak of the laser pulse, and that by significantly improving the temporal contrast, using plasma mirrors, efficient proton acceleration is observed from target foils with thickness less than 50 nm.

Keywords: laser-particle acceleration; proton beam; laser–plasma interactions

1. Background

Ion acceleration driven by intense laser–plasma interactions has been observed for more than two decades. Gitomer *et al.* (1986) provides a review of early ion measurements with long pulse (nanosecond) CO_2 lasers. In these experiments, at focused intensities of approximately $10^{16}\,\mathrm{W\,cm^{-2}}$, protons and carbon ions were accelerated to energies of the order of tens of keV. It was found that the source of the ions was hydro-carbon or water contamination layers on the surfaces of the thin foil targets irradiated by the laser, and that the acceleration mechanism was driven by charge separation within the laser-produced plasma.

In recent years, there has been a renewed interest in laser-driven ion acceleration due to the availability of high-intensity laser pulses (greater than

* Author for correspondence (p.mckenna@phys.strath.ac.uk).

One contribution of 15 to a Discussion Meeting Issue ‘Laser-driven particle acclerators: new sources of energetic particles and radiation’.

10^{18} W cm^{-2}) with sub-picosecond duration, made possible by the introduction of chirped pulse amplification (CPA). Proton acceleration to tens of MeV energies and in low divergent beams of excellent quality has been demonstrated (Clark *et al.* 2000*a*; Snavely *et al.* 2000). Heavier ions have also been observed, with energies up to hundreds of MeV (Clark *et al.* 2000*b*; Hegelich *et al.* 2002). Laser-generated ion beams have a number of desirable properties. It has been shown experimentally that proton beams are generated with low transverse and longitudinal emittance (about 100 fold better than beams produced from typical RF accelerators; Cowan *et al.* 2004). The ions are produced in short bunches of high brightness with a measured efficiency of conversion from laser energy to ions as high as 12% (Snavely *et al.* 2000). An interesting application of laser-driven protons is to probe the evolution of electric fields within a plasma (Borghesi *et al.* 2002). These techniques have even been applied to measure the spatial and temporal evolution of the electrostatic fields responsible for laser-driven ion acceleration. Other proposed applications of this potentially compact ion source include ion radiotherapy (Bulanov *et al.* 2002), isotope production for medical imaging techniques (Ledingham *et al.* 2004) and as injectors for the next generation of ion accelerators (Krushelnick *et al.* 2000). The need to optimize and control ion acceleration for many of these applications has motivated a number of research groups worldwide to investigate laser-driven proton and heavier ion acceleration.

In this paper, we discuss aspects of our present understanding of the mechanisms leading to ion acceleration in the interaction of high-intensity laser pulses with thin foil targets, and highlight examples of some of the recent progress made in this research area. Specifically, we discuss the influence of the temporal contrast of the laser pulse on ion acceleration, and illustrate our discussion with results from an ongoing research campaign on laser-driven proton acceleration at the Lund Laser Centre (LLC) in Sweden.

2. Ion acceleration mechanisms

We begin by noting that the high energy ions that are produced by laser–plasma interactions are not directly accelerated by the laser pulse—this would require much higher focused intensities (greater than 10^{22} W cm^{-2}) than are currently available. Instead, ion acceleration occurs due to the build up of electrostatic fields, resulting from charge separation due to the laser pulse driving electron motion inside the irradiated target. By creating and heating a plasma, the laser pulse drives ion acceleration. Although a variety of target types, including gas, water droplets, clusters, thin foils and thick solid targets, have been used to demonstrate the acceleration of ions (Mendonca *et al.* 2001), the highest quality ion beams are observed with thin foil targets.

When a high-intensity laser pulse is focused onto a surface of a target foil, the leading edge of the laser pulse (or the amplified spontaneous emission (ASE)-pedestal) ionizes the target (at intensities of approximately 10^{12} W cm^{-2}) leading to an expanding plasma, with an exponentially decreasing density at increasing distance from the target surface. The peak of the laser pulse propagates in the expanding plasma until it reaches a critical plasma density (approximately 10^{21} cm^{-3}), at which the plasma frequency (collective electron

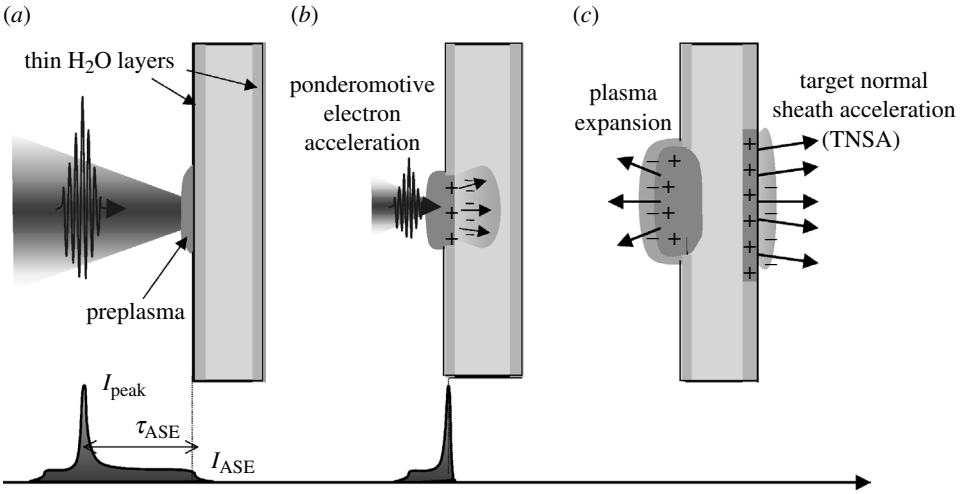

Figure 1. The main ion acceleration mechanisms in the interaction of a high-intensity laser pulse with a thin foil target. (*a*) The ASE-pedestal arriving at the target surface, prior to the peak of the laser pulse, creates a plasma. (*b*) The peak intensity of the laser pulse interacts with the preformed plasma, ponderomotively accelerating electrons into the target and creating a space charge separation, leading to ion acceleration. (*c*) The accelerated electrons emerge from the target rear surface, forming an electron sheath with micron-scale Debye length. The resulting quasi-static electric field, of the order of TV m^{-1}, leads to ionization and ion acceleration to multi-MeV energies (the TNSA mechanism). Plasma expansion at the target front surface leads to ion acceleration in the backward direction.

motion against the ion background) cancels the propagation of an electromagnetic wave. The main laser–plasma interaction occurs at this critical density surface. The plasma electrons react to the ponderomotive potential of the focused laser light, and are pushed from regions of high laser intensity to regions of lower intensity. A number of important electron acceleration mechanisms have been identified. At lower intensities, of the order of 10^{16} W cm^{-2}, and short plasma scale lengths, resonant absorption dominates, leading to electron acceleration in the direction of the density gradient. At higher intensities, greater than 10^{18} W cm^{-2} for laser light at wavelength of approximately 1 μm, relativistic laser–plasma interactions occur. The $\boldsymbol{v}\times\boldsymbol{B}$ component of the Lorentz force then leads to electron acceleration in the laser propagation direction, with electron energies corresponding to MeV temperatures. If a high-intensity, *p*-polarized laser pulse is focused onto a target foil at an angle other than target normal, two distributions of electrons (resulting from the two acceleration mechanisms) will thus be driven into the foil in different directions. This has been demonstrated experimentally (Santala *et al.* 2000; Brandl *et al.* 2003). We also note that in order to sustain large currents of hot electrons moving forward, return currents of cold electrons are produced to overcome the Alfvén limit.

Separation of the accelerated electrons from the ion background within the plasma creates electrostatic fields which accelerate the ions. At least two ion acceleration schemes have been put forward to explain experimental observations, and are summarized in figure 1. Ponderomotive electron acceleration produces an electrostatic field on the laser-irradiated surface, resulting in the

acceleration of ions from the front side of the target, passing through the target and forming a beam in the forward direction (Clark *et al.* 2000*a*). The hot electron populations which are accelerated through the target foil form an electron sheath at the rear surface, resulting in field ionization and ion acceleration—the target normal sheath acceleration model (TNSA; Wilks *et al.* 2001). The quasi-static electric fields (approximately $kT_{\mathrm{hot}}/e\lambda_{\mathrm{D}}$, where kT_{hot} is the hot electron temperature and λ_{D} is the Debye length) can reach values greater than $10^{12}\,\mathrm{V\,m^{-1}}$, leading to ion energies in the MeV range for micron scale Debye lengths. Because of the presence of hydrocarbon and water vapour on the surfaces of the foils (for experiments performed at typical vacuums of approximately 10^{-5} mbar), protons are usually observed in large numbers, and due to their high charge-to-mass ratio they are more efficiently accelerated than heavier ion species and effectively screen the electric acceleration fields experienced by heavier ions. Recent studies have shown that in order to efficiently accelerate heavier ions the proton source layers should be removed from the target foil by heating or ablation (Hegelich *et al.* 2002; McKenna *et al.* 2004). In addition to ion acceleration in the forward direction (direction of laser propagation), we note that plasma expansion at the front surface of the target foil can also lead to ion acceleration in the backward direction. The energies and other properties of accelerated ions depend strongly on the parameters of the charge separation, and this is currently the subject of intense experimental and theoretical research programmes.

3. Effects of laser pulse contrast on ion acceleration

Laser pulse intensity contrast is a measure of the ratio of the intensity of laser light in the peak of the laser pulse to the background intensity. An important contributory factor to the background light is ASE, which is produced when inherent background light gets amplified due to the gain in the amplifying crystals. The ASE forms a pedestal extending of the order of nanoseconds before and after the peak of the laser pulse, as shown schematically in figure 1*a*, where the peak intensity is denoted I_{peak} and I_{ASE} and τ_{ASE} denote the level and duration of the ASE pedestal prior to the peak of the pulse, respectively. The background may also contain pre-pulses arising from, for example, incomplete compression of the CPA pulse through higher order phase errors or spectral clipping. In this discussion article, we specifically consider the effects of the ASE pedestal on ion acceleration.

An ASE-pedestal arriving at the surface of a target foil will generate X-rays which can heat the bulk of the target. If the target foil is sufficiently thin, the target rear surface is radiatively heated. In addition, the ablation pressure due to the arrival of the ASE-pedestal on the surface of the foil launches a shock wave into the target. Again, if the target foil is sufficiently thin for the shock wave to propagate through the foil before the peak of the laser pulse arrives on target, expansion of the target rear surface can result. Both processes can ruin the steep density gradient on the target rear surface required for ion acceleration by the TNSA mechanism.

The optimum target thickness for efficient proton acceleration, without inducing an expansion of the target rear surface, depends not only on the laser pulse parameters, but also the target density. For the purposes of illustrating our

discussion, however, we consider only Al, which has been widely shown to be a suitable target material for efficient proton acceleration. Many of the reported measurements on laser-driven proton acceleration have involved laser pulses with typical contrast in the range 10^5–10^7. As a result, Al target foils with thickness greater than a few microns are usually employed to ensure that the ASE-pedestal does not induce an expansion of the target rear surface (Roth *et al.* 2002). Using laser pulses with contrast of approximately 10^6, for example, Spencer and co-workers (McKenna *et al.* 2002; Spencer *et al.* 2003) observed the highest proton energies from Al target foils of thicknesses of approximately 12 μm, with a sharp cut-off with thinner foils. With pulses of contrast better than 2×10^7, Kaluza *et al.* (2004) have shown that the optimum target thickness for proton acceleration decreases with the duration of the ASE-pedestal—with a minimum pedestal duration of 0.5 ns an optimum Al thickness of 2 μm was observed to produce protons with energies up to ∼3.5 MeV. They further report that with targets below the optimum thickness the spatial profile of the proton beam becomes blurred—consistent with an expansion of the target rear surface.

The expansion of the target rear surface is sensitive to both the level and duration of the ASE-pedestal prior to the peak of the pulse. Let us consider, for example, a laser pulse with a peak focused intensity of 10^{19} W cm^{-2} and with a pedestal duration of 1 ns and intensity of approximately 10^{13} W cm^{-2}. This ASE-pedestal produces an ablation pressure of greater than 2 Mbar and launches a shock wave of velocity ∼10 μm ns^{-1} into an Al target foil. Assuming a constant shock velocity (ignoring expansion of the shock wave within the target), the shock wave will reach the rear surface, of target foils with thickness less than 10 μm, prior to the arrival of the peak of the laser pulse on target and, therefore, the formation of the electron sheath responsible for ion acceleration at the target rear surface. A reduction in the pedestal duration or ASE intensity (resulting in a slower shock wave) reduces the lower limit of the target thickness before shock breakout on the rear surface results.

A pulse contrast of between 10^5 and 10^7 is typical of high-power laser systems. A measurement of proton acceleration with laser pulses with exceptional temporal contrast of 10^{10} was reported (Mackinnon *et al.* 2002) using the JanUSP laser (at the Lawrence Livermore National Laboratory, USA). With this contrast, a dramatic enhancement in measured proton energy was observed when decreasing target thickness below a certain threshold. This was attributed to electron recirculation inside thin foil targets. While the laser pulse is present, electrons generated at the laser focus are reflected from the Debye sheath built up at the target surfaces and recirculate within the target, enhancing the electrostatic fields responsible for ion acceleration. With a peak intensity of 1×10^{20} W cm^{-2}, Mackinnon *et al.* (2002) observed proton energies up to 24 MeV from Al targets with thickness down to 3 μm. Such an enhancement due to recirculation in thin foil targets motivates research using even thinner targets.

In the remainder of this article, we discuss progress made in an ongoing research programme at the Lund Laser Center to investigate proton acceleration as a function of various laser and target parameters. In particular, we discuss a transition window of ASE-pedestal conditions, for which shock breakout modifies the properties of the accelerated ion beam, without resulting in evaporative expansion of the target rear surface. We also discuss a progression towards ion acceleration from ultra-thin targets under ultra-high contrast conditions, facilitated by the use of plasma mirrors.

4. Experimental approach at the Lund Laser Centre

We use the 10 Hz, multi-terawatt, femtosecond laser at the LLC, which can deliver pulses of 1.0 J in 35 fs at a wavelength of 800 nm. The laser system is described elsewhere (Lundh *et al.* in preparation). Importantly, a total of four Pockels cells are used to efficiently suppress any pre-pulses and to facilitate control of the duration of the ASE pedestal, in the range 1.0–4.5 ns. The system is also equipped with an acousto-optic pulse shaper for spectral and temporal control of the seed pulses from the oscillator. The amplitude of the acoustic wave launched into the acousto-optic crystal determines diffraction efficiency of this device. Thereby, the seed energy to the first amplification stage, a regenerative amplifier, can be continuously controlled. Because of its high gain, the bulk of the ASE is produced in the regenerative amplifier. Increasing the seed energy to the amplifier, other things kept constant, lowers the amount of ASE produced by it. The pulse energy from the final amplifier remains unchanged, as it operates in saturation. The temporal contrast is measured in the flat part of the pedestal, approximately 100 ps before the main pulse, using a third order autocorrelator, and the ASE intensity is estimated from the measured contrast and the estimated peak intensity. On the nanosecond timescale, the temporal profile is measured with a fast photo diode and oscilloscope. Figure 2 shows a typical temporal profile of the laser pulse.

The laser pulses are focused onto thin foils at 45° angle of incidence by a $f/3$, off-axis parabolic mirror to a focal spot with a $1/e^2$ focal spot diameter of 7 μm, as illustrated in figure 3. A peak intensity on target exceeding 10^{19} W cm^{-2} is inferred from the measured spot size, pulse energy and pulse duration. Target foils are mounted in a multi-target holder to facilitate systematic investigation of proton acceleration as a function of target parameters. An alternative mode of operation involving a plasma mirror (Ziener *et al.* 2003; Dromey *et al.* 2004), to further extend the contrast range available with this laser, is illustrated in the inset of figure 3.

CR-39 nuclear track detector, which is sensitive to ions, but insensitive to electrons and X-rays, is used to diagnose the spatial distribution of the proton beam in the energy range 0.1–11 MeV (1 mm thick CR-39 plates). A CR-39 plate feeder system (not shown in figure 3) enables the proton beam profiles to be recorded on up to 20 laser shots for each pump down cycle of the target vacuum chamber. The proton stopping power in Al (figure 4*a*) is used to determine the spatial profile of the protons above selected threshold energies. An Al filter mask with increasing thickness (figure 4*b*) is employed directly in front of the detector plates. The filters also serve to stop heavier ions from reaching the CR-39 and protect it from target debris.

Proton energy distribution measurements are made using a Thomson parabola ion spectrometer and two compact magnetic spectrometers (figure 3). For both types of spectrometer the dispersed proton beam is again detected using CR-39, but with a thin Al filter, in direct contact, to remove heavier ions and to slow down fast protons for effective detection and analysis. The spectrometers have a line of sight to the laser focal spot in the plane of the laser beam and the target normal, and can be used at a wide range of angles with respect to the target normal.

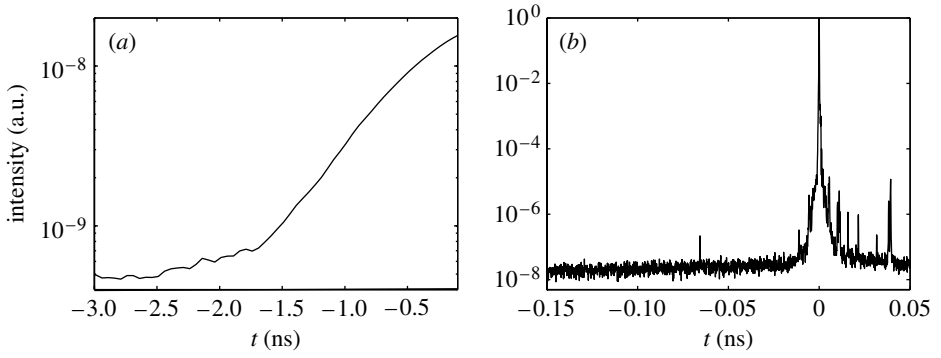

Figure 2. Representative example of temporal profile measurements of the laser pulse, using a fast photo diode (*a*) and a third order autocorrelator (*b*).

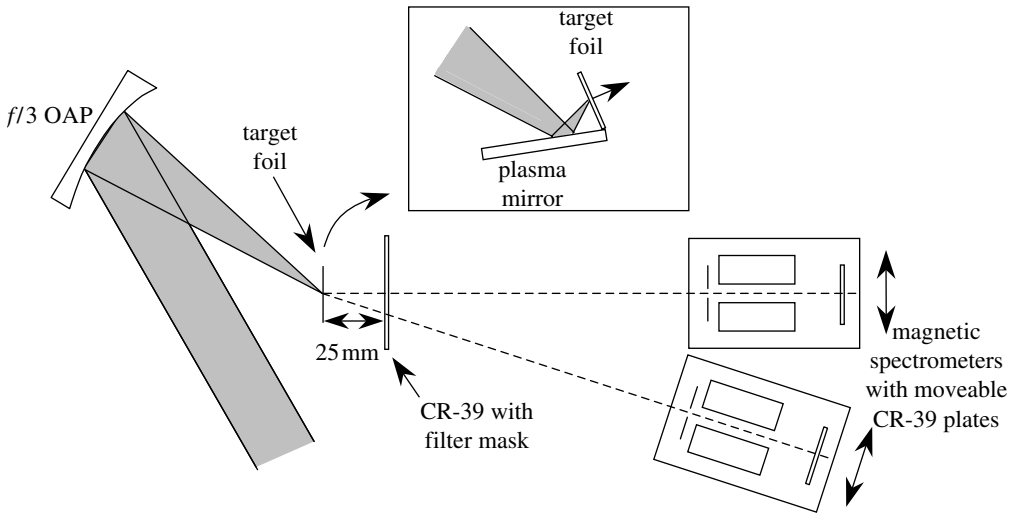

Figure 3. Schematic illustration of the experimental arrangement employed to investigate laser-driven proton acceleration. The spatial and energy distributions of beams of protons accelerated in the forward direction are measured using CR-39 with a filter mask (figure 4) and two magnetic spectrometers and a Thomson parabola spectrometer (not shown). Inset: the addition of a plasma mirror is used to achieve higher laser pulse contrast. The plasma mirror (a glass plate) is positioned such that the intensity of the ASE-pedestal is below the ionization threshold of the glass and is therefore transmitted. A plasma is created by the rising edge of the peak of the laser pulse and reflects the main laser pulse, with the bulk of the energy, onto the target foil.

5. Measured sensitivity of proton emission to ASE-pedestal

We measure proton beam spectral distributions and spatial profiles for a range of target foil thicknesses, as a function of ASE-pedestal intensity and duration. Typically, we observe a broad energy distribution of protons, extending beyond 4.5 MeV. As an example, the proton energy spectrum, emitted along target normal, from a 6 μm Al foil irradiated at a few 10^{19} W cm^{-2} is shown in figure 5. We do not specifically investigate the relative contributions to the measured

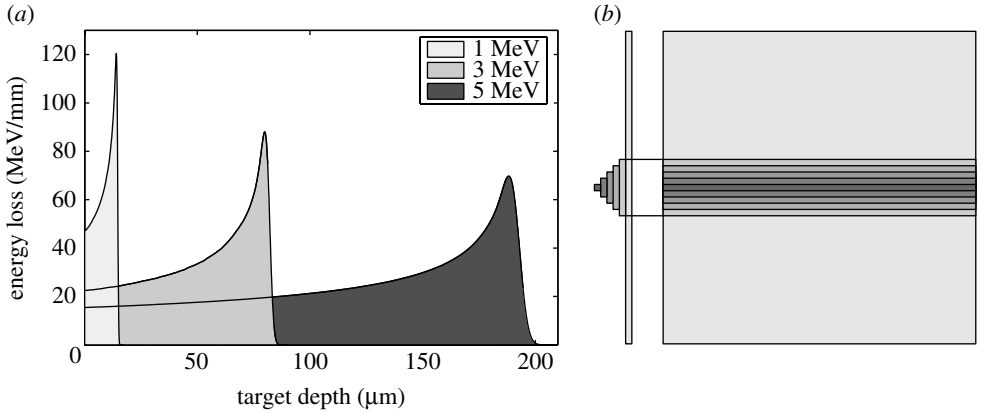

Figure 4. (*a*) Proton stopping powers in aluminium. (*b*) The stepped aluminium filter arrangement placed in front of the CR-39 to enable measurement of the proton spatial distributions above selected energy thresholds.

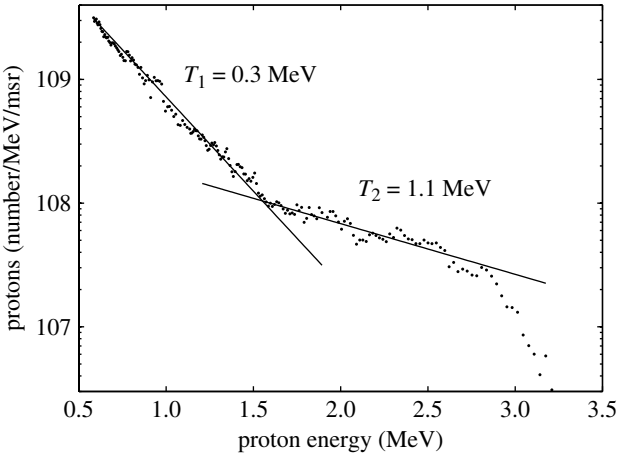

Figure 5. A typical proton energy spectrum, observed by irradiating a 6 μm thick Al foil at a few 10^{19} W cm^{-2}. The spectrum comprises of two Boltzmann-like distributions with temperatures of 0.3 and 1.1 MeV.

proton beam resulting from the front and rear side acceleration mechanisms previously discussed, but note that simulations by Sentoku *et al.* (2003) predict a maximum energy of approximately 7.5 MeV due to the rear surface acceleration process, and less than 1 MeV for protons originating from the front surface, for the 35 fs pulse duration used in this work.

Typical examples of our recordings of the spatial profiles of the proton beam above selected energies, as a function of Al target foil thickness and laser pulse contrast, are summarized in figure 6. We observe that, independent of target thickness, the proton beam is always emitted in the plane of the laser beam and the target normal, and in agreement with previous observations (Snavely *et al.* 2000), we also observe that the angular divergence of the collimated beams decreases with increasing proton energy. Importantly, similar to Kaluza *et al.*

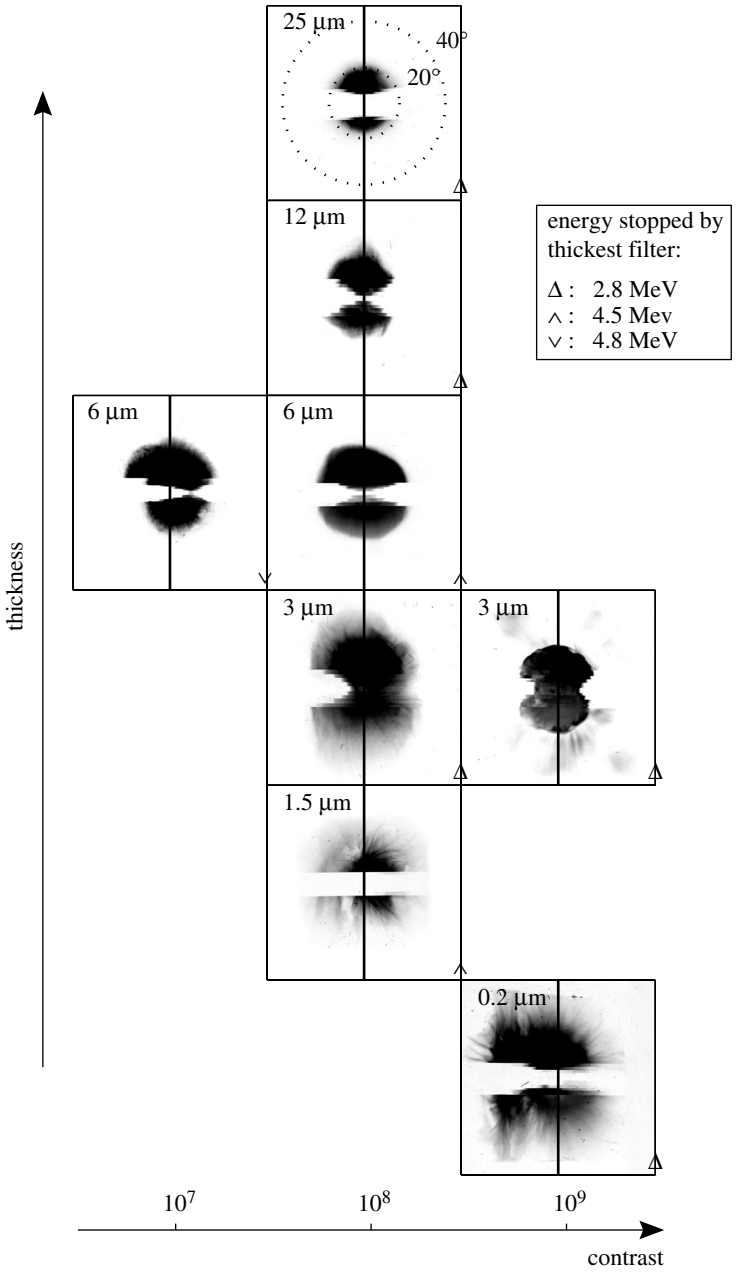

Figure 6. Representative examples of spatial and energy distributions of proton beams, as a function of Al target foil thickness and laser pulse contrast. Al filters, as illustrated in figure 4, are used. The laser pulse contrast of 10^9 was obtained using a plasma mirror with reflectivity of the order of 50%. The two circles, shown for the 25 µm result, correspond to the 20° and 40° half-angles of the divergence of the proton beam, and are applicable to all examples. The vertical lines correspond to the target normal. At laser pulse contrasts of 10^7 and 10^8 it is observed that the high-energy component of the proton beam is shifted away from the target normal, towards the laser direction (to the right of the distribution), for the 6 and 3 µm thick targets, respectively. The angle of deviation is found to increase with proton energy.

(2004), we observe that the optimum target thickness for proton acceleration is sensitive to the duration of the ASE-pedestal. We further observe that it is also sensitive to ASE intensity.

Consider the example profiles recorded with laser pulses of contrast $\sim 10^8$ (with ASE level a few 10^{11} W cm^{-2} and duration 1 ns) in figure 6. We observe proton beams centred on the target normal direction for all proton energies from targets with thickness 6 μm or greater. With the same laser conditions, and with a target thickness of 1.5 μm, we observe a reduction in the homogeneity of the proton beam and begin to observe structure in the beam profile. We also observe a significant reduction in the energy of emitted protons. This is consistent with our understanding that for a sufficiently thin target the ASE-pedestal will ruin the steep density gradient required on the target rear surface for efficient ion acceleration, and that there is an optimum foil thickness for given laser contrast conditions (approximately 3–6 μm for the case considered).

Of particular interest is our reported observation (Lindau *et al.* 2005) that for a certain window of ASE-pedestal conditions we observe a deflection of the high-energy component of the emitted proton beam, away from the target normal and towards the laser direction. This is illustrated in figure 6 for the 6 μm Al target at a laser pulse contrast of 10^7, and 3 μm target at contrast 10^8. The observation is explained in terms of proton acceleration from a target rear surface which is undergoing dynamic expansion due to breakout of the shock wave, launched by the ablation pressure on the front surface by the arrival of the ASE pedestal (Lindau *et al.* 2005). Irradiation of a target foil with *p*-polarized pulses at 45° angle of incidence ponderomotively drives electrons in the laser forward direction, leading to sheath formation in a region of the target rear surface where the localized target normal is directed away from the global target normal. The highest energy protons, produced at the peak of the sheath field are thus accelerated in a direction away from the global target normal. With laser pulses of contrast 10^8, this deviation is not observed for the 6 μm target, but is observed for 3 μm and thinner targets. For 6 μm thick Al foils, we find that threshold ASE-pedestal intensity and duration conditions are reached with laser pulses of contrast between 10^8 and 10^7, corresponding to shock breakout on the rear surface and leading to the observed deflection. For 3 μm thick Al foils the threshold conditions are lower, resulting in the observed high-energy proton deviation with pulses of 10^8 contrast.

Our observations show that a window of ASE conditions exists, for a given target thickness, in which shock break out modifies the spatial distribution of the accelerated proton beam, without destroying the steep density gradient required by the TNSA acceleration mechanism. This model of a dynamic deformation of the target rear surface, induced by a shock wave with Mbar pressures and velocity of the order of μm ns^{-1} is supported by simulations using the hydrodynamic code MULTI (Lundh *et al.* in preparation).

6. Proton acceleration with ultra-high contrast laser pulses

We routinely obtain pulses with a temporal contrast of approximately 1.0×10^8 from the multi-terawatt LLC laser. With this contrast, and a minimum pedestal duration of 1.0 ns, we observe protons with energy extending beyond 4.5 MeV,

from Al target foils of thickness down to 0.2 μm. Motivated by the observed enhancement in proton numbers and energies reported by Mackinnon *et al.* (2002), and attributed to electron recirculation within thin foils, we extend our investigation to even higher contrast and thinner targets.

Enhanced contrast pulses are produced by inserting a plasma mirror (Ziener *et al.* 2003; Dromey *et al.* 2004) into the focusing beam, as illustrated in the inset of figure 3. A planar plasma mirror was operated at 45° in *p*-polarization giving a measured energy reflectivity of 41%. The ASE intensity on the plasma mirror is less than 10^8 W cm^{-2}, which is well below the threshold for plasma formation. By calculating the ratio of ASE reflectivity to main pulse reflectivity, we estimate a contrast enhancement of 45. This leads to a contrast on target of up to 10^{10}.

We find that, by increasing the contrast by more than one order of magnitude, we can decrease the target thickness, for which we observe high energy well-defined proton beams, by more than one order of magnitude (Neely *et al.* in preparation). In fact, with laser pulses with temporal contrast better than 10^9 we observe protons with multi-MeV energies from Al target foils with thickness less than 50 nm. We also find that, as illustrated in figure 6, the increased contrast has the effect of 'switching-off' the proton deviation observed, at a contrast of 10^8, with a 3 μm Al target. This is expected due to the associated reduction in ASE-pedestal intensity and hence the ablation pressure and velocity of the resulting shock wave launched in the target.

7. Summary and future challenges

We conclude that the temporal contrast of the laser pulse plays an important role in laser-driven ion acceleration from thin foil targets. Our experimental programme has led directly to the observation that for a target foil of a given thickness, threshold ASE-pedestal intensities and durations exist, above which an ASE-induced shock wave can lead to non-evaporative deformation of the target rear surface and a resulting change in the direction of proton emission. This observation points to a laser controllable manipulation of the proton beam profile. This is achieved without the need for precision pre-manufactured targets and, therefore, in principle, can be performed at high repetition rates.

In addition, at the start of our research programme we would not have imagined that we would observe well-defined, energetic proton beams from target foils with thickness ranging over 3 orders of magnitude—from 50 μm to below 50 nm. The fact that we observe efficient ion acceleration from ultra-thin targets raises interesting questions regarding the electron transport and ion acceleration processes at work, and opens up exciting directions for our ongoing research programme. We anticipate further experimentation, possibly involving double plasma mirrors, to extend our investigations of the influence of laser contrast on ion acceleration and to elucidate the acceleration mechanisms with even thinner target foils, approaching the skin depth (approximately 8 nm) for 800 nm laser light absorption.

In general, the advances made in understanding the parameters affecting proton acceleration, and to some extent manipulating the proton beam, encourage the view that this potentially compact and unique source of ions may become useful for

a number of potential applications. Further experimental and theoretical research is required to optimize and control laser-driven ions. An important challenge remains to find the parameters which control the accelerated ion energy distribution, to enable high-quality beams of quasi-monoenergetic ions to be produced.

We acknowledge the financial support by the Access to Research Infrastructures activity in the Sixth Framework Programme of the EU (contract RII3-CT-2003-506350, Laserlab Europe) and by the Swedish Research Council. P.McK. acknowledges the award of a Royal Society of Edinburgh Personal Fellowship.

References

Borghesi, M. *et al.* 2002 Electric field detection in laser–plasma interaction experiments via the proton imaging technique. *Phys. Plasmas* **9**, 2214. (doi:10.1063/1.1459457)

Brandl, F., Pretzler, G., Habs, D. & Fill, E. 2003 Cerenkov radiation diagnostics of hot electrons generated by fs–laser interactions with solid targets. *Europhys. Lett.* **61**, 632. (doi:10.1209/epl/i2003-00118-y)

Bulanov, S. V., Esirkepov, T. Z., Khoroshkov, V. S., Kunetsov, A. V. & Pegoraro, F. 2002 Oncological hadrontherapy with laser ion accelerators. *Phys. Lett. A* **299**, 240. (doi:10.1016/S0375-9601(02)00521-2)

Clark, E. L. *et al.* 2000*a* Measurements of energetic proton transport through magnetized plasma from intense laser interactions with solids. *Phys. Rev. Lett.* **84**, 670. (doi:10.1103/PhysRevLett.84.670)

Clark, E. L. *et al.* 2000*b* Energetic heavy-ion and proton generation from ultra-intense laser–plasma interactions with solids. *Phys. Rev. Lett.* **85**, 1654. (doi:10.1103/PhysRevLett.85.1654)

Cowan, T. *et al.* 2004 Ultralow emittance, multi-MeV proton beams from a laser virtual-cathode plasma accelerator. *Phys. Rev. Lett.* **92**, 204 801. (doi:10.1103/PhysRevLett.92.204801)

Dromey, B., Kar, S., Zepf, M. & Foster, P. S. 2004 The plasma mirror—a subpicosecond optical switch for ultrahigh power lasers. *Rev. Sci. Instrum.* **75**, 645. (doi:10.1063/1.1646737)

Gitomer, S. J., Jones, R. D., Begay, F., Ehler, A. W., Kephart, J. F. & Kristal, R. 1986 Fast ions and hot electrons in the laser–plasma interaction. *Phys. Fluids* **29**, 2679. (doi:10.1063/1.865510)

Hegelich, M. *et al.* 2002 MeV ion jets from short–pulse–laser interaction with thin foils. *Phys. Rev. Lett.* **89**, 085 002. (doi:10.1103/PhysRevLett.89.085002)

Kaluza, M., Schreiber, J., Santala, M. I. K., Tsakiris, G. D., Eidmann, K., Meyer-ter-Vehn, J. & Witte, K. J. 2004 Influence of the laser prepulse on proton acceleration in thin-foil experiments. *Phys. Rev. Lett.* **93**, 045 003. (doi:10.1103/PhysRevLett.93.045003)

Krushelnick, K. *et al.* 2000 Ultrahigh-intensity laser-produced plasmas as a compact heavy ion injection source. *IEEE Trans. Plasma Sci.* **28**, 1184. (doi:10.1109/27.893296)

Ledingham, K. W. D. *et al.* 2004 High power laser production of short-lived isotopes for positron emission tomography. *J. Phys. D: Appl. Phys.* **37**, 2341. (doi:10.1088/0022-3727/37/16/019)

Lindau, F., Lundh, O., Persson, A., McKenna, P., Osvay, K., Batani, D. & Wahlström, C.-G. 2005 Laser-accelerated protons with energy dependent beam direction. *Phys. Rev. Lett.* **95**, 175002.

Lundh, O., Lindau, F., McKenna, P., Persson, A. & Wahlström, C.-G. In preparation.

Mackinnon, A. J., Sentoku, Y., Patel, P. K., Price, D. W., Hatchett, S. P., Key, M. H., Andersen, C., Snavely, R. A. & Freeman, R. R. 2002 Enhancement of proton acceleration by hot-electron recirculation in thin foils irradiated by ultraintense laser pulses. *Phys. Rev. Lett.* **88**, 215 006. (doi:10.1103/PhysRevLett.88.215006)

McKenna, P. *et al.* 2002 Characterization of multiterawatt laser–solid interactions for proton acceleration. *Rev. Sci. Instrum.* **73**, 4176. (doi:10.1063/1.1516855)

McKenna, P. *et al.* 2004 Proton and heavier ion acceleration in ultrahigh intensity laser-interactions with heated target foils. *Phys. Rev. E* **70**, 036 405. (doi:10.1103/PhysRevE.70.036405)

Mendonca, J. T., Davies, J. R. & Eloy, M. 2001 Proton and neutron sources using terawatt lasers. *Meas. Sci. Technol.* **12**, 1801.

Neely, D., Foster, P., Lindau, F., Lundh, O., McKenna, P., Persson, A. & Wahlström, C.-G. In preparation.

Roth, M. *et al.* 2002 Energetic ions generated by laser pulses: a detailed study on target properties. *Phys. Rev. Spec. Topics—Accel. Beams* **5**, 061 301. (doi:10.1103/PhysRevSTAB.5.061301)

Santala, M. I. K. *et al.* 2000 Effect of the plasma density scale length on the direction of fast electrons in relativistic laser–solid interactions. *Phys. Rev. Lett.* **84**, 1459. (doi:10.1103/PhysRevLett.84.1459)

Sentoku, Y., Cowan, T. E., Kemp, A. & Ruhl, H. 2003 High energy proton acceleration in interaction of short laser pulse with dense plasma target. *Phys. Plasmas* **10**, 2009. (doi:10.1063/1.1556298)

Snavely, R. A. *et al.* 2000 Intense high-energy proton beams from petawatt-laser irradiation of solids. *Phys. Rev. Lett.* **85**, 2945. (doi:10.1103/PhysRevLett.85.2945)

Spencer, I. *et al.* 2003 Experimental study of proton emission from 60 fs, 200 mJ high rep-rate 'table-top' laser pulses interacting with solid targets. *Phys. Rev. E* **67**, 046 402. (doi:10.1103/PhysRevE.67.046402)

Wilks, S. C. *et al.* 2001 Energetic proton generation in ultra-intense laser–solid interactions. *Phys. Plasmas* **8**, 542. (doi:10.1063/1.1333697)

Ziener, C., Foster, P. S., Divall, E. J., Hooker, C. J., Hutchinson, M. H. R., Langley, A. J. & Neely, D. 2003 Specular reflectivity of plasma mirrors as a function of intensity, pulse duration, and angle of incidence. *J. Appl. Phys.* **93**, 768. (doi:10.1063/1.1525062)